NEOPLASIA
www.neoplasia.com
Volume 22 Number 10 October 2020 pp. 511-521

Prostate cancer-derived MMP-3 controls intrinsic cell growth and extrinsic angiogenesis

Jeremy S. Frieling; **Tao Li**; **Marilena Tauro**; **Conor C. Lynch** *

Department of Tumor Biology, H. Lee Moffitt Cancer Center & Research Institute, Tampa, FL 33612, USA

Abstract

Bone metastatic prostate cancer significantly impacts patient quality of life and overall survival, and despite available therapies, it is presently incurable with an unmet need for improved treatment options. As mediators of tumor progression, matrix metalloproteinases (MMPs) can degrade extracellular matrix components and regulate growth factor and cytokine bioactivity. Depending on tissue context, MMPs can either promote or inhibit tumorigenesis. Therefore, it is essential to study individual MMPs in specific cancer contexts and microenvironments to support the design and application of selective MMP inhibitors. Here we report that tumor-derived MMP-3 contributes to bone metastatic prostate cancer progression via intrinsic and extrinsic routes. MMP-3 ablation in prostate cancer cell lines significantly reduced *in vitro* growth combined with lowered AKT and ERK phosphorylation and total VEGFR1 and FGFR3 protein levels. *In vivo*, MMP-3 ablated tumors grew at a slower rate and were significantly less vascularized. Quantitative PCR analyses of wild type and MMP-3 silenced prostate cancer cells also demonstrate downregulation of a wide array of angiogenic factors. The extrinsic role for MMP-3 in angiogenesis was supported by *in vitro* endothelial tube formation assays where the lack of MMP-3 in prostate cancer conditioned media resulted in slower rates of tube formation. Taken together, our results suggest that tumor-derived MMP-3 contributes to prostate cancer growth in bone. These data indicate that selective inhibition of MMP-3 and/or targeting MMP generated products could be efficacious for the treatment of prostate to bone metastases.

Neoplasia (2020) 22 511–521

Keywords: Matrix metalloproteinase, Bone, Metastasis, Angiogenesis, Prostate cancer, MMP-3

Introduction

Prostate cancer is the second most prevalent cancer in men in the United States, with 31,620 deaths predicted this year [1]. The men who succumb to the disease typically have evidence of bone metastasis, where the cancer cells thrive by hijacking resident bone cells involved in the skeletal remodeling process, namely osteoblasts and osteoclasts, to generate a growth promoting microenvironment [2]. The resultant metastatic lesions are hallmarked by an irregular pathology of bone formation and destruction, resulting in intense pain, bone fractures, hypercalcemia, and increased patient mortality [3]. At present, there is an unmet need to further elucidate the biological mechanisms that permit prostate cancer growth in the bone in order to improve patient outcomes.

Given the rate of bone matrix remodeling, it is unsurprising that many enzymes capable of extracellular matrix (ECM) processing are highly expressed in the bone-tumor microenvironment. While cathepsin K (cysteine protease) is responsible for osteoclast resorption activity, matrix metalloproteinases (MMPs) are also highly expressed in this setting. MMPs are classically involved with cancer invasion and metastasis, leading to the development of inhibitors that largely failed early clinical trials due to a lack of understanding the complexity of MMP biology, which has been the subsequent research focus [4–7]. For example, depending on tissue context, MMPs can be either pro- or anti-tumorigenic given the extracellular matrix (ECM) or non-ECM substrates that are processed [4,8–12]. MMP-3 serves as a case in point, where when expressed by breast cancer cells it promotes progression [13,14], but in skin carcinogenesis has been shown to be protective by promoting the influx of leukocytes [15]. Several cytokines and growth factors are implicated in the regulation of MMP-3 via DNA response elements within its promoter region, including activator binding protein-1 (AP-1) [16–19]. Notably, a polymorphism identified 1171 bp upstream of the transcription start site where differences in adenosine content (5A versus 6A) has been shown to influence promoter activity [20] and may be associated with increased aggressiveness of several cancers, including prostate [21–24]. We previously noted high MMP-3 expression at the prostate tumor-bone interface [4], and this expression of MMP-3 by metastatic prostate cancer cells was confirmed in human bone biopsies. Here we examined whether, in the context of bone meta-

* Corresponding author at: H. Lee Moffitt Cancer Center & Research Institute, 12902 USF Magnolia Dr., SRB-3, Tampa, FL 33612, USA.
e-mail address: conor.lynch@moffitt.org (C.C. Lynch).

https://doi.org/10.1016/j.neo.2020.08.004

static prostate cancer, tumor-derived MMP-3 would protect or promote disease progression.

In the current study, we demonstrate that tumor-derived MMP-3 contributes to *in vitro* prostate cancer cell growth as well as *in vivo* tumor growth in an intratibial model of bone metastasis. Histologically, the MMP-3 ablated intratibial tumors displayed a significant decrease in vasculature compared to control tumors. Furthermore, MMP-3 ablated prostate cancer cells showed decreased angiogenic capabilities via a number of measurements *in vitro* and *in vivo*. Together these data suggest that MMP-3 contributes both intrinsically and extrinsically to prostate cancer growth in bone by regulating molecular pathways associated with mitogenic and angiogenic cellular processes.

Materials and methods

Cell lines and culture

The PAIII cell line was a generous gift from the University of Notre Dame [25]. The PC-3M-luc-C6 cell line was purchased from Caliper Life Sciences. C4-2B were a generous gift from Leland Chung group [26]. LNCaP (Cat #CRL-1740) and HUVEC (Cat #CRL-1730) were purchased from the ATCC. All cell lines were periodically mycoplasma tested (#25237, LiliF Diagnostics) and short tandem repeat (STR) verified at the Moffitt Clinical Translational Research Core. Cell lines were passaged in recommended culture medium supplemented with 10% fetal calf serum. For MMP-3 ablation, either siRNA or shRNA were used. Human-specific siRNA were purchased from Origene (Cat #SR302926) and transfected transiently (Lipofectamine® RNAiMAX, Invitrogen, #13778-075) following the manufacturer's instructions. Rat-specific shRNA constructs were purchased from Origene (Cat #HC144224). Stable transfection of shRNA was achieved using standard transfection protocols (Superfect, Qiagen, #301305) followed by selection with puromycin. For analysis of growth in MMP-3 ablated cell lines, either MTS (C4-2B, PC-3M, and HUVEC) or luciferase growth titer (PAIII) assays were used. Cell lines were plated in 96-well plates at 2×10^4 cells per well. Viability was measured at 24, 48, and 72 h time points, following the manufacturers' provided protocols (CellTiter 96, #G5421, Promega; Luciferase Assay System, #E1501, Promega).

In vivo studies

Mice were purchased from Jackson Laboratory (Bar Harbor, ME). All animal experiments were performed with IACUC approval (R1762, CCL) and in accordance with the guidelines set forth in the *Guidelines for the Care and Use of Laboratory Animals* published by the National Institutes of Health. 6-week old male Rag $2^{-/-}$ mice were intratibially injected with luciferase-expressing PAIII control or shMMP-3 Clone 01 cell lines (5×10^4 cells). Contralateral limbs were injected with saline as a control for injury. Mice were imaged for bioluminescence twice weekly as a correlate of tumor growth (IVIS™ 200, Perkin Elmer). Luciferin was administered intraperitoneally (150 mg/kg body weight) and incubated for 10 min prior to acquisition to reach signal plateau. At endpoint (1×10^6 RLU average), hind limbs were collected following carbon dioxide euthanasia and fixed overnight in 10% neutral buffered formalin. Tumors that grew outside of bone (as determined by H&E staining) were excluded from all final analyses.

Radiographic images (Faxitron, X-ray Corp) were obtained using energy of 35 kVp and an exposure time of 8 ms with a spatial resolution of 10 lp/mm (48 μm). Lesion area was calculated as a function of the total area of the tibial medullary canal using ImageJ software. For μCT analysis, the proximal tibia metaphyses were scanned (μCT-40; Scanco Medical). An evaluation of trabecular bone structural parameters was performed in a 1000 μm region beginning 500 μm distally from the growth plate. A three-dimensional cubical voxel model of bone was constructed from which calculations were derived for relative bone volume per total volume and trabecular number [27].

Gene expression analyses

For standard qPCR, RNA was extracted with TRIzol® according to manufacturer's instructions (Invitrogen #15596). cDNA reverse transcription was performed using a High Capacity cDNA Reverse Transcription Kit (Applied Biosystems, #4368813). The concentrations of cDNA samples were determined by NanoDrop, and equal amounts used for PCR by HotStarTaq Master Mix (Qiagen, #203445). Reactions were prepared using SYBR Green PCR Master Mix (Applied Biosystems, #4309155). Primer sequences for genes of interest are as follows: Rat MMP-3 Forward 5′-GATGGTATTCAATCCCTCTATGG-3′; Rat MMP-3 Reverse 5′-A ACAAGACTTCTCCCCGCAG-3′; Human MMP-3 Forward 5′-AGG CAAGACAGCAAGGCATA-3′; Human MMP-3 Reverse 5′-GGTTCA TGCTGGTGTCCTCA-3′; 18S Forward 5′-GTAACCCGTTGAACCC CATT-3′; 18S Reverse 5′-CCATCCAATCGGTAGTAGCG-3′; GAPDH Forward 5′-CCTGCACCACCAACTGCTTA-3′; GAPDH Reverse 5′-CCACGATGCCAAAGTTGTCA-3′. A panel of 84 angiogenesis-related genes was studied using a mouse specific osteogenesis RT^2 Profiler™ Assay (Qiagen, PARN-024ZA-6). RNA was extracted by Trizol® and subsequently purified using an RNeasy MinElute Cleanup kit (Qiagen, #74204). Reverse transcription was performed using an RT^2 First Strand Kit (Qiagen, #330401). PCR array plates were run on standard qPCR instruments (ABI Prism 7900HT) and analyzed with online software (http://www.SABiosciences.com/pcrarraydataanalysis.php). Fold change for all qPCR experiments was calculated using delta delta CT (ΔΔCT) method [28].

Histology and immunostaining

Mouse tissues were fixed overnight in 10% neutral buffered formalin. Tibias were decalcified for 21 days in a solution of 14% EDTA at 4 °C, replacing the solution every 3 days, and then processed and paraffin embedded following standard protocols. Formalin fixed, paraffin embedded tissues were sectioned at a thickness of 5 μm. Human samples of prostate to bone metastasis were a generous gift from Dr. Colm Morrissey and the University of Washington.

All formalin-fixed paraffin-embedded sections were dewaxed and rehydrated to water before staining. Sections were stained with hematoxylin and eosin to observe gross anatomy and/or trichrome to measure bone formation. Trichrome staining was used to identify areas of trabecular bone formation (blue/green staining of type I collagen). Briefly, slides were incubated in Bouin's solution for 10 min at 55 °C, rinsed in water, and counterstained with hematoxylin. Slides were then incubated in Gomori's trichrome solution for 20 min and differentiated in fresh 0.5% acetic acid for 2 min. After rinsing in water, slides were dehydrated and coverslipped. Bone area to total area (B.Ar./T.Ar.) and tumor areas were determined by measuring trabecular bone volume within a 1.0 mm long area beginning 0.5 mm distal from the growth plate using ImageJ software [29].

For immunofluorescence, antigen retrieval was performed by heat (Tris EDTA buffer, pH 8.0, in pressure cooker, 5 min). Slides were blocked in 10% goat serum in 1× TBS for 1 h at room temperature. Primary antibodies (MMP-3, Triple Point Biologics RH-MMP-3, 1:100; pan-Cytokeratin, Sigma #C2562, 1:500; Phospho-Histone H3, Millipore #06-570, 1:200; Cleaved Caspase 3, Cell Signaling #9664S, 1:300; FGFR3, Cell Signaling #4574S, 1:200; VEGFR1, abcam #32152, 1:300; Von Willebrand Factor, Dako A0082, 1:250) were diluted in 10% goat serum and incubated overnight at 4 °C in a humidified cham-

ber. After 3 washes in 1X TBST followed by 1 wash in 1× TBS, secondary antibodies (Alexa Fluor™ Goat Anti Rabbit 568, Thermo Fisher Scientific #A-11011; Alexa Fluor Goat Anti Mouse 488, Thermo Fisher Scientific #A32723) were incubated at a 1:1000 dilution in 10% normal goat serum for 1 h at room temperature. Slides were rinsed with DAPI solution (1 μg/mL in TBS), washed three times in 1× TBS, and mounted using aqueous solution (AquaMount #13800). Slides were stored in the dark at 4 °C until micrograph acquisition. A minimum of three representative images per section were acquired for each tissue. Cleaved caspase 3, phospho-Histone H3, and Von Willebrand Factor staining micrographs were quantified using ImageJ to count the number of positive cells and/or areas of positive staining. FGFR3 and VEGFR1 intensity were quantified where co-localized with pan-Cytokeratin using Definiens Tissue Studio.

Immunoblotting

Cells were lysed with cold RIPA (150 mM NaCl, 1 mM EDTA, 1% Triton X-100, 1% sodium deoxycholate, 0.1% SDS, 20 mM Tris pH 8) containing protease and phosphatase inhibitor (Thermo Scientific, #78442) using standard procedures. Total protein concentration was determined using BCA (Pierce, #23225), and an equal amount of total protein was loaded in SDS–PAGE gel. Blots were blocked in 5% BSA for 1 h, followed by 3 × 10 min washes in 1× TBST. Primary antibody for phospho-ERK (Cell Signaling Technology #9101; diluted 1:1000 in blocking solution + 0.1% Tween-20), ERK (Cell Signaling Technology #4695; diluted 1:1000 in blocking solution + 0.1% Tween-20), phospho-AKT (Cell Signaling Technology #9275S, diluted 1:1000 in blocking solution + 0.1% Tween-20), AKT (Cell Signaling Technology #4691S, diluted 1:1000 in blocking solution + 0.1% Tween-20), FGFR3 (Cell Signaling Technology #4574S, diluted 1:1000 in blocking solution + 0.1% Tween-20), or VEGFR1 (Abcam #32152, diluted 1:1000 in blocking solution + 0.1% Tween-20) was incubated overnight at 4 °C. The blots were washed 3 × 10 min in 1× TBST and incubated with HRP-conjugated anti-species secondary (Cell Signaling Technology, Rabbit #7074/Mouse #7076, diluted 1:1000 in blocking solution). Blots were developed using enhanced chemiluminescence (Pierce #32106) or ultra-sensitive chemiluminescence (Pierce #34096) and visualized using a LI-COR Odyssey Fc Imaging System. β-Actin (Cell Signaling Technology #3700S; diluted 1:1000 in blocking solution + 0.1% Tween-20) was used as standard loading control.

Endothelial cell tube formation assay

For tube formation assays, 24-well tissue culture plates were coated with 200 μL of 10 mg/mL Growth Factor Reduced Matrigel Matrix Basement Membrane (Corning #354230) and incubated at 37 °C for 1 h. HUVEC cells (3×10^4) were then overlaid and incubated in the presence of conditioned media from PAIII control or PAIII shMMP-3 cells. FBS-free DMEM was used as a negative control, and F12K medium containing 10% FBS was used as a positive control. Images were acquired at 1, 2, 6, 12, and 24 h after cell seeding. A minimum of three fields of view per well were captured at each timepoint, and the length of tubes were measured and quantified using ImageJ.

Migration assay

For migration assays, HUVEC migration was assessed using modified Boyden chamber assay. Cells were seeded (5.0×10^5) in the upper chamber after 24 h serum starvation. PAIII conditioned media were added to the lower chamber and incubated over a 6 h period at 37 °C. FBS-free DMEM and DMEM + 1% FBS were used as negative and positive controls, respectively. Chamber filters were excised, and the migrated cells were stained with hematoxylin. The number of migrated cells was determined by counting 3 random fields at 20× for each condition, in triplicate.

Statistical analysis

To determine statistical significance among groups, *T*-test or analysis of variance (ANOVA) followed by Tukey's multiple comparison test was performed. A p-value <0.05 was considered as statistically significant. Data are presented as standard error from the mean (S.E.M). All statistical analyses were performed with Graph Pad Prism 8.4.2 (GraphPad Inc., LaJolla, CA).

Results

MMP-3 expression is localized to prostate cancer cells in bone metastatic disease

To determine the clinical relevance of MMP-3 in prostate cancer, we initially assessed *MMP-3* expression in publically accessible human prostate cancer gene sets. Gene sets comparing normal prostate tissue to carcinoma were interrogated using Oncomine (www.oncomine.org), and we noted that *MMP-3* expression was elevated in multiple datasets (Fig. 1A) [30–32]. These datasets often do not include metastatic disease, we therefore acquired human tissue specimens of prostate to bone metastases from the University of Washington Rapid Warm Body Autopsy Program (Dr. Colm Morrissey) and co-stained using immunofluorescence for pan-cytokeratin and MMP-3. Of the nine patient samples analyzed, eight showed predominant expression of MMP-3 in the prostate tumor cells compared to the stromal surroundings (Fig. 1B). Based on these findings, we focused on determining the role of cancer cell-derived MMP-3 in a panel of human (LNCaP, C4-2B, and PC3M) and rodent (PAIII) prostate cancer cell lines for *MMP-3* expression by PCR and noted positive expression of the *MMP-3* transcript in all (Fig. 1D). Together, these data demonstrate that elevated levels of MMP-3 exist in prostate cancer, including in patients with prostate to bone metastases, and that prostate cancer cells are a predominant source of MMP-3 in the prostate tumor-bone microenvironment.

MMP-3 silencing inhibits prostate tumor growth in bone

To interrogate the effects of prostate cancer-derived MMP-3, we generated stable MMP-3 knockdown PAIII cell lines using RFP-expressing, small hairpin RNA (shRNA) constructs. Two independent PAIII shMMP-3 clones with different knockdown efficiency were selected for further *in vitro* study and comparison to a scrambled shRNA control (Fig. 2A). Using bioluminescence as a read out, we first asked if there was any difference in cell proliferation and noted that the MMP-3 ablated cells grew significantly more slowly over time compared to controls (Fig. 2B). We observed that MMP-3 ablation using siRNA also significantly impacted the growth of human prostate cancer cell lines (LNCaP, C4-2B, PC3M) (Supplemental Fig. S1). The effect of MMP-3 ablation on proliferation suggested decreased mitogenic signaling. This was found to be the case when we analyzed levels of phosphorylated AKT and extracellular signal-regulated kinases (ERK) (Fig. 2C). Similarly, decreases in phosphorylated AKT and ERK were observed in the PC3M cells when MMP-3 was transiently suppressed via siRNA transfection (Supplemental Fig. S1).

MMP-3 can process an array of growth factors and cytokines [4,33–39]. We next examined whether the anti-proliferative effect of MMP-3 ablation *in vitro* would be recapitulated *in vivo*. Given the consistent and significant level of *MMP-3* knockdown (Fig. 2A), we performed these

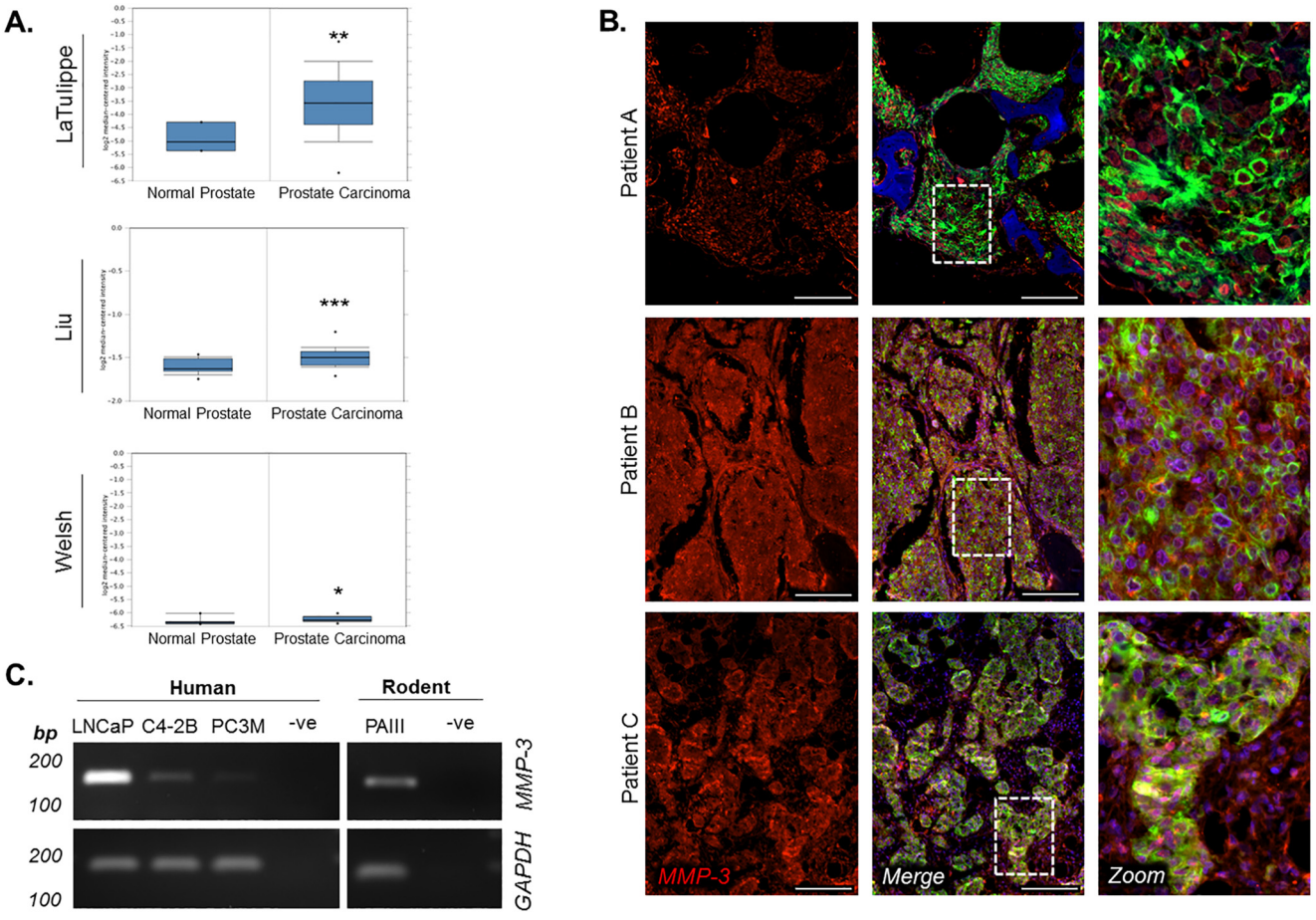

Fig. 1. MMP-3 expression is localized to prostate cancer cells in bone metastatic disease. (A) Comparison of *MMP-3* expression in normal vs. cancerous prostate tissue queried in LaTulippe, Liu, and Welsh datasets [30–32] from Oncomine (www.oncomine.org). (B) Representative fluorescent micrographs depicting MMP-3 localization in human bone metastatic prostate cancer (n = 9; scale bar = 200 μm) Dashed white box indicates area of magnification in rightmost panels. (C) PCR confirming *MMP-3* expression in human and rodent prostate cancer cell lines. *GAPDH* used as reference gene. Molecular weight markers are indicated in base pairs (bp). Asterisks denote statistical significance ($^*p < 0.05$, $^{**}p \leq 0.01$, $^{***}p \leq 0.001$).

studies using the PAIII shMMP-3 Clone 01 cells. To mimic bone metastatic disease, luciferase-expressing PAIII control and shMMP-3 cells (5×10^4, n = 10 per group) were injected directly into the tibias of 6 week old, male immunocompromised $Rag2^{-/-}$ mice. Contralateral limbs were injected with an equivalent volume of saline as a control for injury in *ex vivo* bone histomorphometry analyses. We have previously shown that the PAIII model rapidly produces mixed osteolytic/osteogenic responses over the course of approximately 15 days prior to breaching the cortical bone [27,40,41]. Using bioluminescence measurements as a correlate of tumor growth, we observed that PAIII shMMP-3 tumors grew at a significantly slower rate compared to the control group in bone (Fig. 2D). Consistent with these results, histological quantification of proliferative (phosphorylated histone H3) and apoptotic (cleaved caspase 3) indices within these *in vivo* tumors revealed a significant reduction in proliferation and a significant increase in apoptosis (Fig. 2E and F). We also measured tumor volume in trichrome stained sections. Consistent with our bioluminescence data, we observed a decrease in tumor volume in the MMP-3 knockdown group compared to the controls (Supplemental Fig. S2; p = 0.058). Although not statistically significant, we posit that this may be due to differences in the stromal architecture/composition of the tumors in each group using this particular method. Taken together however, ablation of MMP-3 clearly reduced prostate cancer cell growth in bone.

We also examined the effects of MMP-3 ablation in prostate cancer cells on the surrounding bone microenvironment. To this end, we performed *ex vivo* X-ray and high resolution micro computed tomography (μCT) imaging to measure the degree of osteolysis and osteogenesis, respectively. Interestingly, there were no significant changes noted (Supplemental Fig. S2). These data were further confirmed by histomorphometry analysis of trichrome stained sections (Supplemental Fig. S2). Therefore, despite regulating tumor growth, tumor-derived MMP-3 does not appear to impact cancer-induced bone disease in this model.

MMP-3 ablation suppresses vascularization of prostate tumors in bone

In processing the bone tissues, we also noted differences in vascularization. To investigate this further, we performed immunofluorescence staining using Von Willebrand Factor (VWF) as a readout for vascularization (Fig. 3A). Quantification of the areas of VWF positive staining within pan-cytokeratin co-stained tumors indicated that there was significantly less VWF staining in PAIII shMMP-3 tumors compared to controls (Fig. 3A and B). These data suggest that there is a delay or reduction in angiogenesis as a result of MMP-3 ablation in the prostate cancer cells. As angiogenesis is essential for sustained tumor growth, the reduced vascularization in MMP-3 ablated tumors likely further contributed to the can-

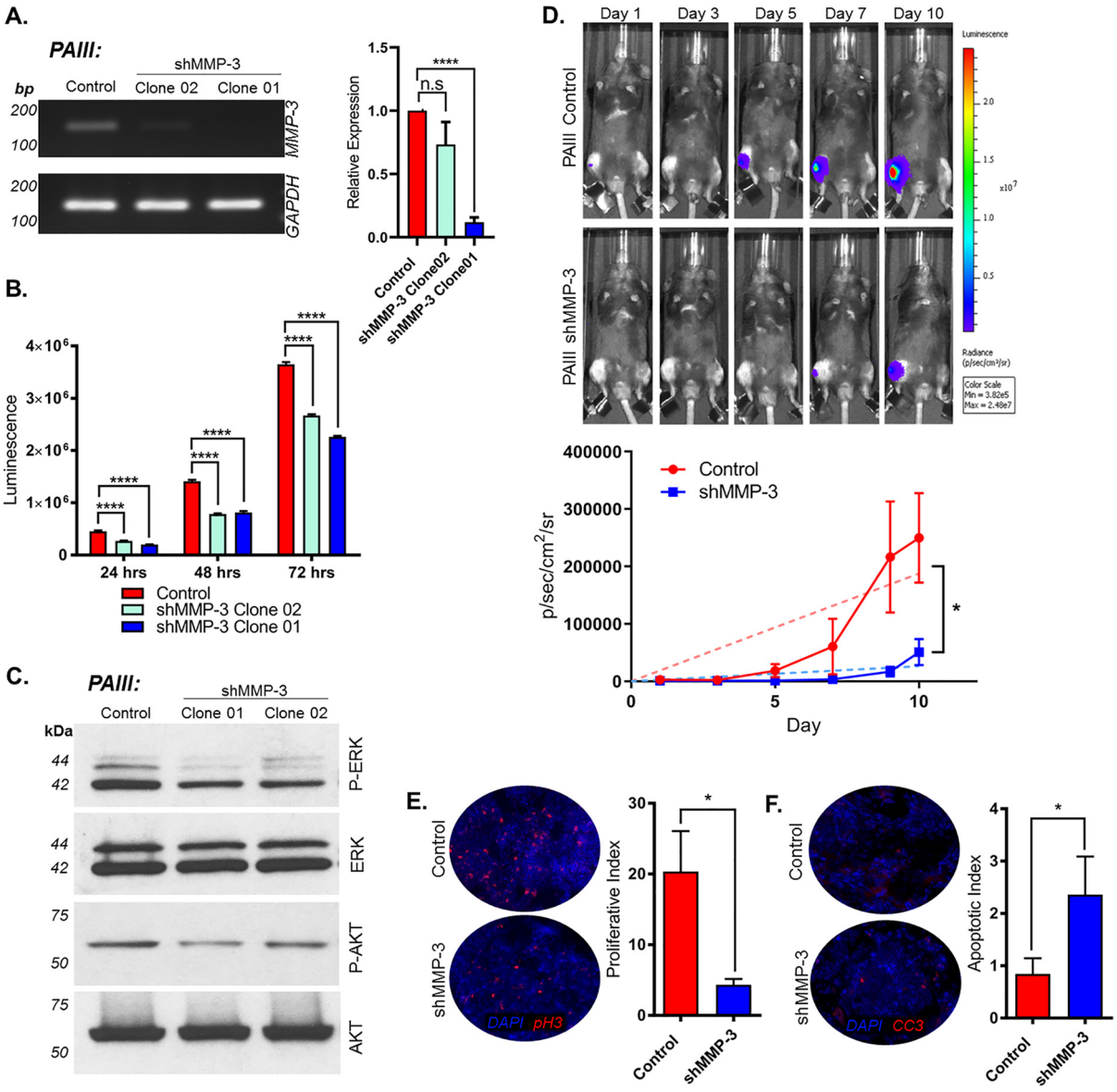

Fig. 2. *MMP-3* silencing inhibits prostate tumor growth in bone. (A) PCR and qPCR demonstrating stable knockdown of *MMP-3* in two independent PAIII clones. *GAPDH* used as reference gene. Molecular weight markers are indicated in base pairs (bp). (B) PAIII control and shMMP-3 cell line growth determined by luminescence assay and relative light unit (RLU) measurement. (C) Western blot analysis of phospho-ERK and phospho-AKT in PAIII control and shMMP-3 cell lines compared to total ERK and AKT, respectively. Molecular weights are shown in kDa. (D) Representative images of *in vivo* bioluminescence for PAIII control and shMMP-3 growth over time (n = 5/group). Graph demonstrates average luminescence for each group. (E and F) *Ex vivo* analyses of proliferative and apoptotic indices at study endpoint using phospho-Histone H3 (pH3, (E)) and Cleaved Caspase 3 (CC3, (F)), respectively. Asterisks denote statistical significance (*$p < 0.05$, ****$p \leq 0.0001$).

cer cell intrinsic effects on growth, resulting in the significant decrease observed *in vivo*.

MMP-3 silencing regulates the transcription of angiogenic genes

Previous studies have described roles for MMP-3 and other MMP family members in regulating angiogenesis [42–45]. To further validate the effects of cancer cell-derived MMP-3 on angiogenesis and vascularization specifically in the PAIII model, we performed a PCR array (Qiagen) to evaluate the expression of 84 unique angiogenesis-related genes in RNA isolated from PAIII control and PAIII shMMP-3 cell lines. Using a ΔΔCT method of data analysis and 2-fold regulation cut off, we noted 38 downregulated genes in the MMP-3 knockout cells, including *CXCL9* (−14.26), *Kdr* (−8.26), *Igf1* (−8.08), *FGFR3* (−5.61), *FGF1* (−3.72), and *MMP-2* (−3.2). Many of these factors may contribute to extrinsic angiogenic processes but also to intrinsic cancer cell proliferation [46–49] (Fig. 3C). Interestingly, *Jag1*, which encodes the Notch ligand Jagged1, was the only significantly upregulated (+2.09) gene identified using the recommended analysis parameters. *MMP-3* was the most downregulated (−14.8), further validating the *MMP-3* knockdown in the PAIII cell line. A STRING analysis predicted candidate signaling reactome pathways specific to our differentially regulated genes, principally those mediated by receptor tyrosine kinases (RTKs) such as PI3K/AKT and MAPK (Fig. 3D). We observed changes in these pathways during initial efforts to characterize the PAIII

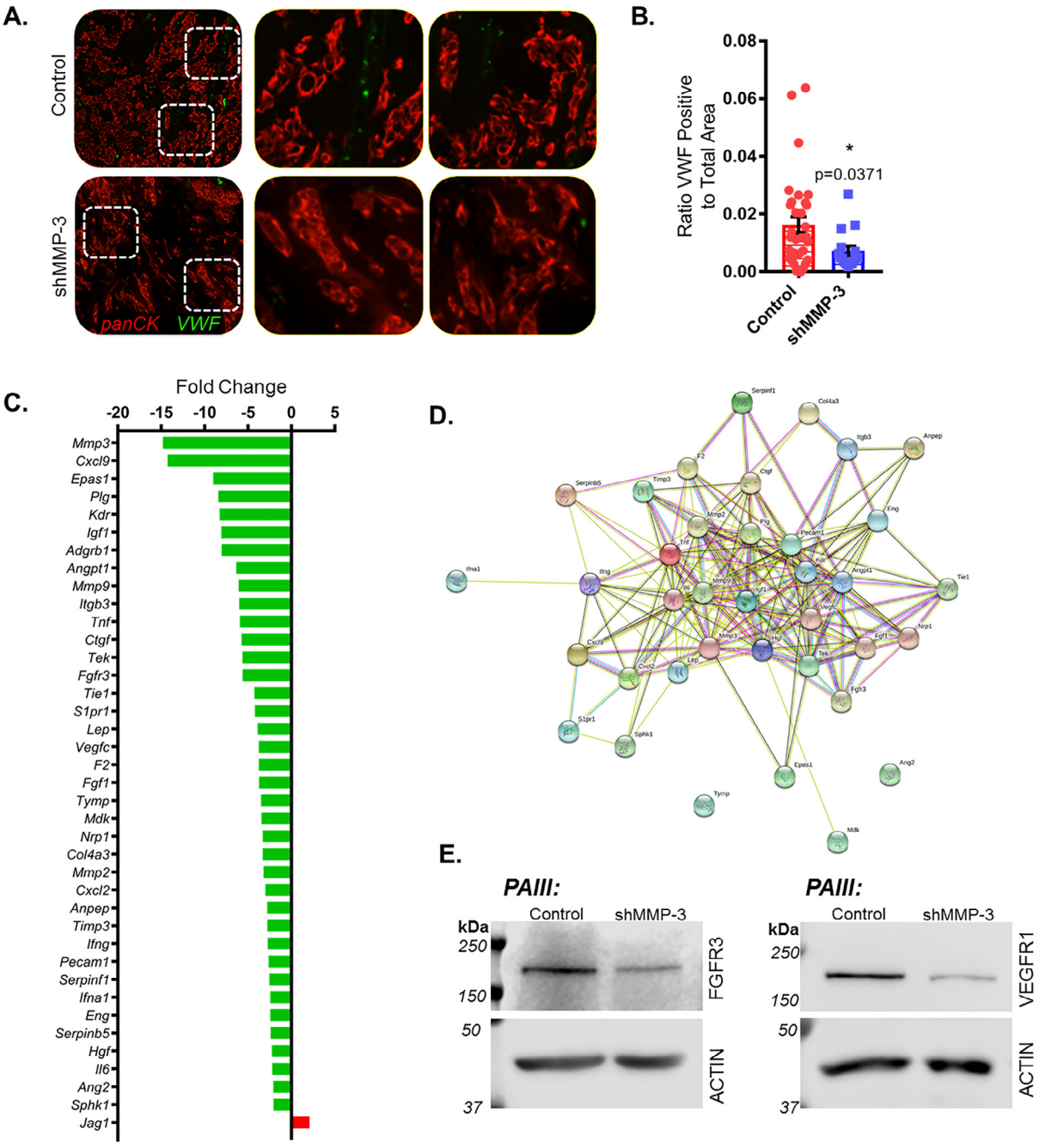

Fig. 3. *MMP-3* ablation suppresses vascularization of prostate tumors in bone and angiogenic gene transcription. (A) Representative fluorescent micrographs depicting Von Willebrand Factor (VWF, green) staining in PAIII control ($n = 6$) and shMMP-3 ($n = 3$) tumors in bone. Pan-Cytokeratin (panCK, red) was used to visualize prostate cancer cells. Dashed boxes indicate magnified areas to the right. (B) VWF positive stained areas were quantified from multiple tissue sections per mouse ($n > 3$) per group and calculated as a ratio to total tumor area. (C) PCR array comparing PAIII control and shMMP-3 gene expression. Fold change calculated by using ΔΔCT method applying a 2-fold cut off. Green indicates decreased expression, red increased expression compared to control. (D) Protein–protein interaction network (STRING) of proteins corresponding with PCR array output genes. (E) Western blot validation of decreased FGFR3 and VEGFR1 signaling receptors in PAIII control and shMMP-3. β-Actin was used as a loading control. Molecular weights are shown in kDa. Asterisks denote statistical significance ($^*p < 0.05$).

shMMP-3 cell lines as evidenced by decreased phosphorylation of AKT and ERK (Fig. 2C), and the STRING output further confirmed the predominant changes in biological activity we noted in MMP-3 ablated PAIII cells. To further develop the findings of the PCR array and STRING analysis, we focused on the expression of the cell surface receptors implicated in activation of these signaling pathways. Here we consistently noted decreased expression of VEGFR1 and FGFR3 (Fig. 3E).

MMP-3 ablation reduces FGFR3 expression in vivo

To validate the impact of MMP-3 ablation on VEGFR1 and FGFR3 we interrogated the expression of both proteins via by immunofluorescence staining of *ex vivo* tissue sections (Fig. 4A and B). We noted positive VEGFR1 staining in both tumor and stroma (Fig. 4A), whereas FGFR3 expression was predominantly localized to the tumor cells (Fig. 4B).

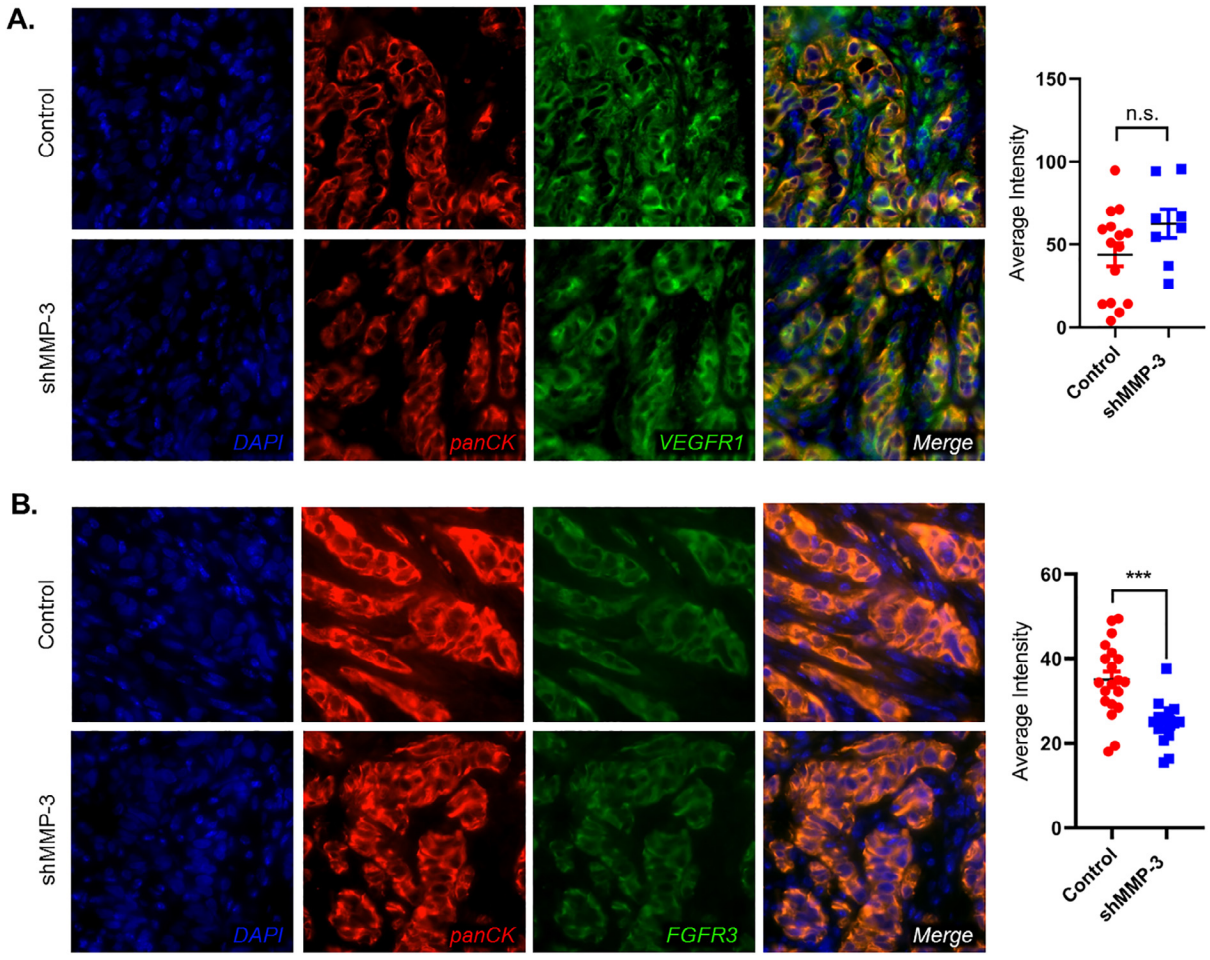

Fig. 4. *MMP-3* ablation reduces FGFR3 but not VEGFR1 expression *in vivo*. (A) Representative fluorescence micrographs demonstrating pan-Cytokeratin (panCK, red) and VEGFR1 (green) staining in PAIII control and shMMP-3 tumors in bone. VEGFR1 intensity in panCK positive prostate cancer cells was measured in multiple fields of view and graphed (right). (B) Representative fluorescence micrographs demonstrating pan-Cytokeratin (panCK, red) and FGFR3 (green) staining in PAIII control and shMMP-3 tumors in bone. FGFR3 intensity in panCK positive prostate cancer cells was measured in multiple fields of view and graphed (right). Asterisks denote statistical significance ($^{***}p \leq 0.001$).

Tumor cell-specific signal intensity for either VEGFR1 or FGFR3 was quantified by Definiens Tissue Studio software. Consistent with *in vitro* findings of PAIII, FGFR3 was significantly decreased in MMP-3 ablated tumors. No differences in VEGFR1 expression were detected in the prostate cancer cells but this analysis could have been confounded by the strong positivity for VEGFR1 noted in the stromal compartment.

Loss of MMP-3 restricts endothelial tube formation

To further test the effect of prostate cancer cell-derived MMP-3 on angiogenesis, we performed an *in vitro* endothelial tube formation assay where human umbilical vascular endothelial cells (HUVEC) were seeded in Matrigel in the presence of conditioned media collected from PAIII control or shMMP-3 cell lines. Endothelial cell tubes began to form in both the PAIII control and shMMP-3 treated groups within the first few hours of culture, whereas tubes in serum free condition (negative control) lagged behind (Fig. 5A). Quantification of the average length of these early tubes revealed that there was no difference between groups at the 6 and 12 h time points. However, at later time points approaching 24 h, the PAIII shMMP-3 conditioned media treated HUVEC formed tubes significantly slower compared to control (Fig. 5B).

We also examined the effect of MMP-3 ablation on HUVEC growth and migration but observed no statistically significant overall differences (Fig. 5C and D). We did observe a small decrease in ERK phosphorylation in HUVEC overlaid with PAIII shMMP-3 conditioned media compared to media from PAIII control cells, however there was no difference in AKT phosphorylation (Fig. 5E). Together, these findings demonstrated that prostate cancer-derived MMP-3 impacts the expression of angiogenic factors and contributes to the vascularization of the prostate cancer-bone microenvironment.

Discussion

Bone metastasis remains a prevalent and clinically challenging aspect of advanced prostate cancer. Understanding how the disease progresses in the skeleton can yield novel therapeutic targets. Here, we show that tumor-derived MMP-3 contributes to metastatic prostate tumor growth in bone both *in vitro* and *in vivo*. *In vitro* studies revealed that the reduced growth rate was accompanied by a decrease in ERK and AKT phosphorylation and lower overall VEGFR1 and FGFR3 expression, while *ex vivo* analysis of the intratibial tumors demonstrated that MMP-3 ablation not only resulted in a reduced tumor growth rate but also less vascularization.

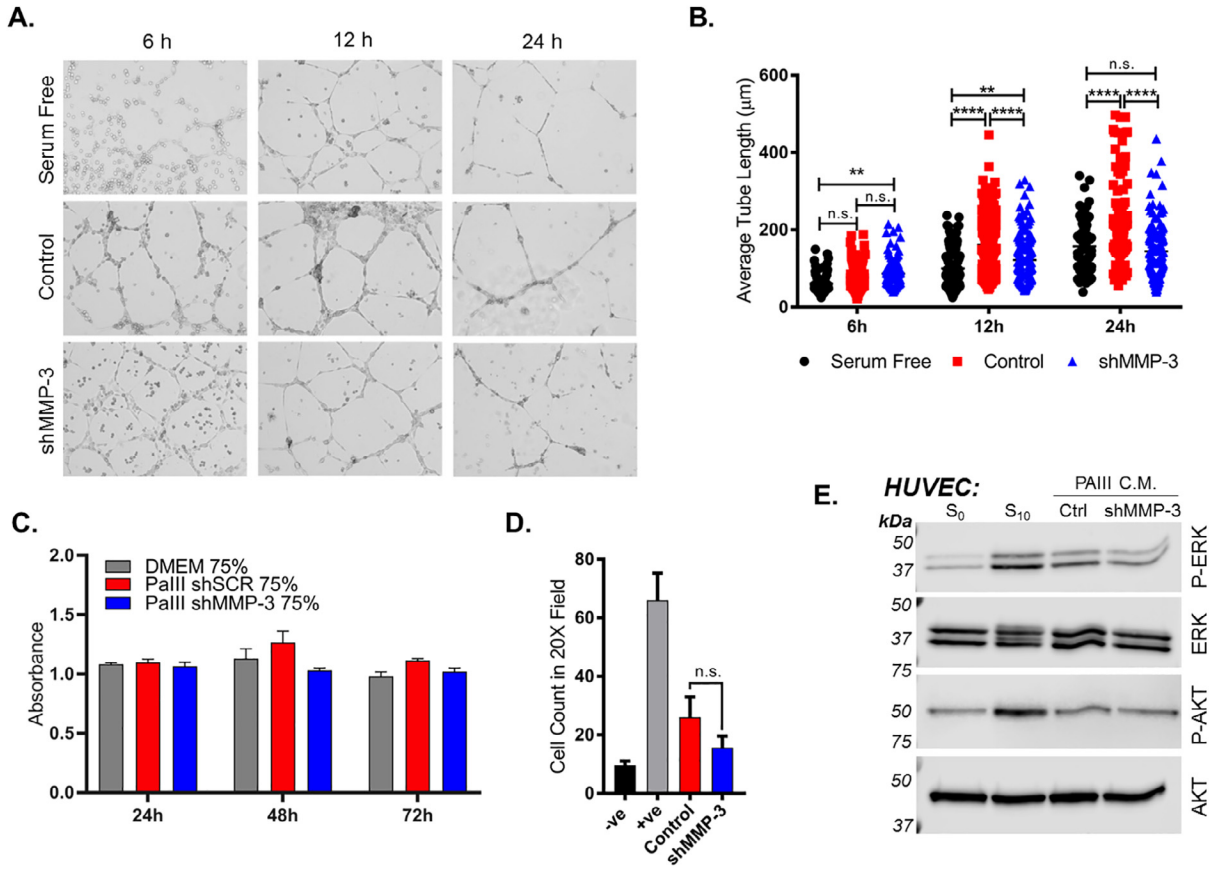

Fig. 5. MMP-3 contributes to endothelial cell tube formation *in vitro*. (A) Representative micrographs depicting endothelial cell (HUVEC) tube formation in the presence of CM from PAIII control and shMMP-3 cells at 6 h, 12 h, and 24 h time points. (B) Quantification of average length of endothelial tube (ImageJ) from three fields of view per condition per time point. (C) Impact of conditioned media derived from PAIII control or *MMP-3* silenced cells on HUVEC growth. MTT absorbance was used as a readout for cell growth. (D) HUVEC migration to CM from PAIII. Number of H&E stained HUVEC per filter were quantified after 6 h incubation. (E) Western blot assaying induction of phospho-ERK and phospho-AKT in HUVEC in response to CM from PAIII control and shMMP-3 compared to total ERK and AKT, respectively. Molecular weights are shown in kDa. Asterisks denote statistical significance (**$p \leq 0.01$, ****$p \leq 0.0001$). n.s. indicates not significant.

We further verified the impact of MMP-3 on angiogenesis *in vitro*, showing an inhibition of endothelial cell tube formation in HUVEC treated with conditioned media from MMP-3 ablated prostate cancer cells and *in vivo*, demonstrating reduced FGFR3 expression in MMP-3 ablated prostate tumors in bone. We did not observe reduced expression of VEGR1 in MMP-3 ablated bone metastatic prostate cancer cells *in vivo* but this was difficult to measure due to the strong stromal positivity for the receptor. Analyses of VEGFR1 expression at earlier time points during tumor establishment and growth may be more informative. Taken together, our findings suggest that MMP-3 contributes to bone metastatic prostate cancer by both intrinsic (tumor cell growth) and extrinsic (angiogenesis) mechanisms.

MMP-3 can possess either contributory or protective roles in cancer, depending on the tumor context [13,15,50]. Here we show that prostate cancer-derived MMP-3 promotes disease progression in bone. These findings are consistent with former studies of MMP-3 in different cancer contexts [51–54]. To our knowledge, our findings presented here are the first to directly examine the impact of cancer-derived MMP-3 on prostate tumor growth in bone. Few studies have examined MMP-3 in prostate cancer, and those that have done so, focused on primary disease. Consistent with our observations in bone, these studies have reported that MMP-3 contributes to primary disease progression by mechanisms such as promoting invasion and migration [54] and modulating angiogenesis [53]. With respect to bone, a recent study reported that heightened MMP-3 expression driven by Notch3 enhanced the development of prostate cancer-induced osteoblastic bone lesions [55]. Notably, when MMP-3 was inhibited in this model, the formation of osteoblastic metastases was abrogated. Although we did not note any differences in cancer-induced bone disease, the intratibial PAIII model used in our studies takes approximately two weeks to complete, and it is possible that differences in osteogenesis would be more apparent in slower progressing models.

MMPs regulate signaling and tumorigenesis via several methods, including degradation of extracellular matrix and processing of mitogenic and angiogenic factors [56]. MMP-3 is also known to cleave several non-matrix substrates such as insulin growth factor binding protein 3 (IGFBP3) [42,57], latent transforming growth factor β binding proteins (LTBP) [34,58], and heparin binding epidermal growth factor-like growth factor (HB-EGF) [33]. Extracellular matrix bound fibroblast growth factor (FGF) has also shown to be released by MMP-3. Specifically, losing the association with perlecan resulted in lower affinity toward FGF receptors since perlecan functions as a co-receptor [59]. Notably, we observed decreased expression of FGFR3 protein in the cell lines where MMP-3 was ablated, suggesting that the FGF/FGFR axis is involved in our models. MMP-3 has also been reported in the literature as being an important regulator of angiogenesis. For example, MMP-3 cleaves a complex consisting of CTGF and VEGF (165) to promote the pro-angiogenic activity of

VEGF [43]. MMP-3 can also cleave a matrix-associated protein called Secreted Protein Acidic And Rich In Cystein (SPARC), generating novel polypeptides that regulate endothelial cell proliferation and migration *in vitro* [44], necessary steps during angiogenesis [60]. Underscoring the complexity of MMP biology and the diverse roles for MMPs from different cellular source and tissue contexts, there is at least one report where MMP-3 negatively impacts angiogenesis by mediating the degradation of VEGFR2, however these observations were not made in the presence of a reactive tumor-bone microenvironment [61]. In this regard, it should be noted, that our studies focused on cancer derived MMP-3, but the protease is also expressed by other bone stromal cells such as osteoblasts. The contribution of bone stromal MMP-3 to prostate cancer progression in bone remain to be determined [62].

Other MMPs, particularly MMP-2 and MMP-9, have often been associated with mitogenic and angiogenic activities in cancer. For example, MMP-9 can drive prostate tumor growth in bone by promoting angiogenesis [8]. The ability of MMPs to activate latent MMPs and proteases is well known, and MMP-3 may also contribute to cell growth and tumor angiogenesis in such a manner. ProMMP-9 is an MMP-3 substrate, which would lead to the active MMP-9 enzyme [63]. Several MMPs, including MMP-3, can also function via non-catalytic mechanisms according to recent reports [64–67]. The MMP-3 hemopexin domain in particular can mediate activities such as epithelial outgrowth, invasion, and branching via interacting or sequestering other proteins [66,67]. Although we have not explored the particular domains responsible for the growth and angiogenesis effects in bone metastatic prostate, novel non-catalytic roles could exist in this context as well.

Elucidating the activities of individual MMPs, such as MMP-3 in bone metastatic prostate cancer, yields valuable information as the field continues to reassess which MMPs should be inhibited in disease and in what context. The majority of MMP inhibitors to date have focused on targeting catalytic domains, however these tend to be well conserved across the MMP family and therefore reduce inhibitor selectivity while increasing toxicity due to broad spectrum activity [68]. New approaches such as targeting enzyme exosites or sub site pockets show promise for the continued development of next generation, ``ultraselective'' MMP inhibitors [69–71]. More recently, work combining a bisphosphonate backbone with an MMP inhibitor has produced bone seeking MMP inhibitors for selective delivery of MMP-2 inhibitor to the tumor-bone microenvironment, thereby circumventing off-target effects [72,73].

In conclusion, we have shown that tumor-derived MMP-3 contributes to prostate cancer growth in bone, both intrinsically and extrinsically. While the direct inhibition of MMP-3 may be difficult due to contrasting activities, the development of selective, bone-seeking MMP-3 inhibitors or the targeting of specific MMP generated products could be efficacious for the treatment of prostate to bone metastases.

CRediT authorship contribution statement

Jeremy S. Frieling: Conceptualization, Methodology, Investigation, Visualization, Writing - original draft, Writing - review & editing. **Tao Li:** Investigation. **Marilena Tauro:** Investigation. **Conor C. Lynch:** Conceptualization, Methodology, Writing - review & editing, Supervision.

Acknowledgements

This work has been supported in part by the Analytic Microscopy Core Facility and Small Animal Imaging Laboratory at the H. Lee Moffitt Cancer Center & Research Institute, an NCI designated Comprehensive Cancer Center.

Funding

This work was supported by the National Cancer Institute, United States (R01CA143094-CCL).

Declarations of Interest

None.

Appendix A. Supplementary data

Supplementary data to this article can be found online at https://doi.org/10.1016/j.neo.2020.08.004.

References

1. American Cancer Society, Cancer Facts & Figures 2020. 2020..
2. Mundy GR. Mechanisms of bone metastasis. *Cancer* 1997;**80**(8 Suppl):1546–56.
3. Bubendorf L et al. Metastatic patterns of prostate cancer: an autopsy study of 1,589 patients. *Hum Pathol* 2000;**31**(5):578–83.
4. Lynch CC et al. MMP-7 promotes prostate cancer-induced osteolysis via the solubilization of RANKL. *Cancer Cell* 2005;**7**(5):485–96.
5. Winding B et al. Synthetic matrix metalloproteinase inhibitors inhibit growth of established breast cancer osteolytic lesions and prolong survival in mice. *Clin Cancer Res* 2002;**8**(6):1932–9.
6. Bonfil RD et al. Inhibition of human prostate cancer growth, osteolysis and angiogenesis in a bone metastasis model by a novel mechanism-based selective gelatinase inhibitor. *Int J Cancer* 2006;**118**(11):2721–6.
7. Coussens LM, Fingleton B, Matrisian LM. Matrix metalloproteinase inhibitors and cancer: trials and tribulations. *Science* 2002;**295**(5564):2387–92.
8. Bruni-Cardoso A et al. Osteoclast-Derived Matrix Metalloproteinase-9 Directly Affects Angiogenesis in the Prostate Tumor-Bone Microenvironment. *Mol Cancer Res* 2010.
9. Thiolloy S et al. An osteoblast-derived proteinase controls tumor cell survival via TGF-beta activation in the bone microenvironment. *PLoS ONE* 2012;**7**(1) e29862.
10. Thiolloy S et al. Osteoclast-derived matrix metalloproteinase-7, but not matrix metalloproteinase-9, contributes to tumor-induced osteolysis. *Cancer Res* 2009;**69**(16):6747–55.
11. Balbin M et al. Loss of collagenase-2 confers increased skin tumor susceptibility to male mice. *Nat Genet* 2003;**35**(3):252–7.
12. Pozzi A et al. Elevated matrix metalloprotease and angiostatin levels in integrin alpha 1 knockout mice cause reduced tumor vascularization. *Proc Natl Acad Sci U S A* 2000;**97**(5):2202–7.
13. Sternlicht MD et al. The stromal proteinase MMP3/stromelysin-1 promotes mammary carcinogenesis. *Cell* 1999;**98**(2):137–46.
14. Thomasset N et al. Expression of autoactivated stromelysin-1 in mammary glands of transgenic mice leads to a reactive stroma during early development. *Am J Pathol* 1998;**153**(2):457–67.
15. McCawley LJ et al. A protective role for matrix metalloproteinase-3 in squamous cell carcinoma. *Cancer Res* 2004;**64**(19):6965–72.
16. Buttice G, Quinones S, Kurkinen M. The AP-1 site is required for basal expression but is not necessary for TPA-response of the human stromelysin gene. *Nucleic Acids Res* 1991;**19**(13):3723–31.
17. Quinones S et al. Transcriptional regulation of human stromelysin. *J Biol Chem* 1989;**264**(14):8339–44.
18. Kerr LD, Holt JT, Matrisian LM. Growth factors regulate transin gene expression by c-fos-dependent and c-fos-independent pathways. *Science* 1988;**242**(4884):1424–7.
19. McDonnell SE, Kerr LD, Matrisian LM. Epidermal growth factor stimulation of stromelysin mRNA in rat fibroblasts requires induction of proto-oncogenes c-fos and c-jun and activation of protein kinase C. *Mol Cell Biol* 1990;**10** (8):4284–93.
20. Ye S et al. Preliminary report: genetic variation in the human stromelysin promoter is associated with progression of coronary atherosclerosis. *Br Heart J* 1995;**73**(3):209–15.

21. Srivastava P, Kapoor R, Mittal RD. Impact of MMP-3 and TIMP-3 gene polymorphisms on prostate cancer susceptibility in North Indian cohort. *Gene* 2013;**530**(2):273–7.
22. Ghilardi G et al. A single nucleotide polymorphism in the matrix metalloproteinase-3 promoter enhances breast cancer susceptibility. *Clin Cancer Res* 2002;**8**(12):3820–3.
23. Hinoda Y et al. Association of functional polymorphisms of matrix metalloproteinase (MMP)-1 and MMP-3 genes with colorectal cancer. *Int J Cancer* 2002;**102**(5):526–9.
24. Zinzindohoue F et al. Single nucleotide polymorphisms in MMP1 and MMP3 gene promoters as risk factor in head and neck squamous cell carcinoma. *Anticancer Res* 2004;**24**(3b):2021–6.
25. Pollard M, Luckert PH. Transplantable metastasizing prostate adenocarcinomas in rats. *J Natl Cancer Inst* 1975;**54**(3):643–9.
26. Wu TT et al. Establishing human prostate cancer cell xenografts in bone: induction of osteoblastic reaction by prostate-specific antigen-producing tumors in athymic and SCID/bg mice using LNCaP and lineage-derived metastatic sublines. *Int J Cancer* 1998;**77**(6):887–94.
27. Cook LM et al. Predictive computational modeling to define effective treatment strategies for bone metastatic prostate cancer. *Sci Rep* 2016;**6**:29384.
28. Livak KJ, Schmittgen TD. Analysis of relative gene expression data using real-time quantitative PCR and the 2(-Delta Delta C(T)) Method. *Methods* 2001;**25**(4):402–8.
29. Helfrich MH, Ralston S. Bone research protocols*Methods in molecular medicine*. Totowa, N.J.: Humana Press; 2003. p. 448.
30. Welsh JB et al. Analysis of gene expression identifies candidate markers and pharmacological targets in prostate cancer. *Cancer Res* 2001;**61**(16):5974–8.
31. LaTulippe E et al. Comprehensive gene expression analysis of prostate cancer reveals distinct transcriptional programs associated with metastatic disease. *Cancer Res* 2002;**62**(15):4499–506.
32. Liu P et al. Sex-determining region Y box 4 is a transforming oncogene in human prostate cancer cells. *Cancer Res* 2006;**66**(8):4011–9.
33. Suzuki M et al. Matrix metalloproteinase-3 releases active heparin-binding EGF-like growth factor by cleavage at a specific juxtamembrane site. *J Biol Chem* 1997;**272**(50):31730–7.
34. Maeda S et al. Activation of latent transforming growth factor beta1 by stromelysin 1 in extracts of growth plate chondrocyte-derived matrix vesicles. *J Bone Miner Res* 2001;**16**(7):1281–90.
35. Imai K et al. Degradation of decorin by matrix metalloproteinases: identification of the cleavage sites, kinetic analyses and transforming growth factor-beta 1 release. *Biochem J* 1997;**322**(Pt 3):809–14.
36. Lochter A et al. Matrix metalloproteinase stromelysin-1 triggers a cascade of molecular alterations that leads to stable epithelial-to-mesenchymal conversion and a premalignant phenotype in mammary epithelial cells. *J Cell Biol* 1997;**139**(7):1861–72.
37. Noe V et al. Release of an invasion promoter E-cadherin fragment by matrilysin and stromelysin-1. *J Cell Sci* 2001;**114**(Pt 1):111–8.
38. Agnihotri R et al. Osteopontin, a novel substrate for matrix metalloproteinase-3 (stromelysin-1) and matrix metalloproteinase-7 (matrilysin). *J Biol Chem* 2001;**276**(30):28261–7.
39. Gearing AJ et al. Matrix metalloproteinases and processing of pro-TNF-alpha. *J Leukoc Biol* 1995;**57**(5):774–7.
40. Luhach I et al. Rapid ex vivo imaging of PAIII prostate to bone tumor with SWIFT-MRI. *Magn Resonan Med* 2013.
41. Araujo A et al. An integrated computational model of the bone microenvironment in bone-metastatic prostate cancer. *Cancer Res* 2014;**74**(9):2391–401.
42. Fowlkes JL et al. Regulation of insulin-like growth factor (IGF)-I action by matrix metalloproteinase-3 involves selective disruption of IGF-I/IGF-binding protein-3 complexes. *Endocrinology* 2004;**145**(2):620–6.
43. Hashimoto G et al. Matrix metalloproteinases cleave connective tissue growth factor and reactivate angiogenic activity of vascular endothelial growth factor 165. *J Biol Chem* 2002;**277**(39):36288–95.
44. Sage EH et al. Cleavage of the matricellular protein SPARC by matrix metalloproteinase 3 produces polypeptides that influence angiogenesis. *J Biol Chem* 2003;**278**(39):37849–57.
45. Zou X et al. The role of matrix metalloproteinase-3 in the doxycycline attenuation of intracranial venous hypertension-induced angiogenesis. *Neurosurgery* 2018;**83**(6):1317–27.
46. Huang B et al. Osteoblasts secrete Cxcl9 to regulate angiogenesis in bone. *Nat Commun* 2016;**7**:13885.
47. Katoh M, Nakagama H. FGF receptors: cancer biology and therapeutics. *Med Res Rev* 2014;**34**(2):280–300.
48. Cohen P et al. Insulin-like growth factors (IGFs), IGF receptors, and IGF-binding proteins in primary cultures of prostate epithelial cells. *J Clin Endocrinol Metab* 1991;**73**(2):401–7.
49. Liang Y, Brekken RA, Hyder SM. Vascular endothelial growth factor induces proliferation of breast cancer cells and inhibits the anti-proliferative activity of anti-hormones. *Endocr Relat Cancer* 2006;**13**(3):905–19.
50. Witty JP et al. Decreased tumor formation in 7,12-dimethylbenzanthracene-treated stromelysin-1 transgenic mice is associated with alterations in mammary epithelial cell apoptosis. *Cancer Res* 1995;**55**(7):1401–6.
51. Robichaud N et al. Phosphorylation of eIF4E promotes EMT and metastasis via translational control of SNAIL and MMP-3. *Oncogene* 2015;**34**(16):2032–42.
52. Banik D et al. MMP3-mediated tumor progression is controlled transcriptionally by a novel IRF8-MMP3 interaction. *Oncotarget* 2015;**6**(17):15164–79.
53. Slavin S et al. Estrogen receptor alpha in cancer-associated fibroblasts suppresses prostate cancer invasion via modulation of thrombospondin 2 and matrix metalloproteinase 3. *Carcinogenesis* 2014;**35**(6):1301–9.
54. Zhu F et al. Eotaxin-1 promotes prostate cancer cell invasion via activation of the CCR3-ERK pathway and upregulation of MMP-3 expression. *Oncol Rep* 2014;**31**(5):2049–54.
55. Ganguly SS et al. Notch3 promotes prostate cancer-induced bone lesion development via MMP-3. *Oncogene* 2020;**39**(1):204–18.
56. Sternlicht MD, Bissell MJ, Werb Z. The matrix metalloproteinase stromelysin-1 acts as a natural mammary tumor promoter. *Oncogene* 2000;**19**(8):1102–13
57. Fowlkes JL et al. Matrix metalloproteinases degrade insulin-like growth factor-binding protein-3 in dermal fibroblast cultures. *J Biol Chem* 1994;**269**:25742–6.
58. Maeda S et al. The first stage of transforming growth factor beta1 activation is release of the large latent complex from the extracellular matrix of growth plate chondrocytes by matrix vesicle stromelysin-1 (MMP-3). *Calcif Tissue Int* 2002;**70**(1):54–65.
59. Whitelock JM et al. The degradation of human endothelial cell-derived perlecan and release of bound basic fibroblast growth factor by stromelysin, collagenase, plasmin, and heparanases. *J Biol Chem* 1996;**271**(17):10079–86.
60. Ausprunk DH, Folkman J. Migration and proliferation of endothelial cells in preformed and newly formed blood vessels during tumor angiogenesis. *Microvasc Res* 1977;**14**(1):53–65.
61. Abdul Muneer PM et al. The mechanisms of cerebral vascular dysfunction and neuroinflammation by MMP-mediated degradation of VEGFR-2 in alcohol ingestion. *Arterioscler Thromb Vasc Biol* 2012;**32**(5):1167–77.
62. Kusano K et al. Regulation of matrix metalloproteinases (MMP-2, -3, -9, and -13) by interleukin-1 and interleukin-6 in mouse calvaria: association of MMP induction with bone resorption. *Endocrinology* 1998;**139**(3):1338–45.
63. Ogata Y, Enghild JJ, Nagase H. Matrix metalloproteinase 3 (stromelysin) activates the precursor for the human matrix metalloproteinase 9. *J Biol Chem* 1992;**267**(6):3581–4.
64. Sakamoto T, Seiki M. Cytoplasmic tail of MT1-MMP regulates macrophage motility independently from its protease activity. *Genes Cells* 2009;**14**(5):617–26.
65. Redondo-Munoz J et al. Matrix metalloproteinase-9 promotes chronic lymphocytic leukemia b cell survival through its hemopexin domain. *Cancer Cell* 2010;**17**(2):160–72.
66. Kessenbrock K et al. A role for matrix metalloproteinases in regulating mammary stem cell function via the Wnt signaling pathway. *Cell Stem Cell* 2013;**13**(3):300–13.
67. Correia AL et al. The hemopexin domain of MMP3 is responsible for mammary epithelial invasion and morphogenesis through extracellular interaction with HSP90beta. *Genes Dev* 2013;**27**(7):805–17.

68. Hadler-Olsen E et al. Regulation of matrix metalloproteinase activity in health and disease. *FEBS J* 2011;**278**(1):28–45.
69. Overall CM. Matrix metalloproteinase substrate binding domains, modules and exosites. Overview and experimental strategies. *Methods Mol Biol* 2001;**151**:79–120.
70. Overall CM, Lopez-Otin C. Strategies for MMP inhibition in cancer: innovations for the post-trial era. *Nat Rev Cancer* 2002;**2**(9):657–72.
71. Dufour A, Overall CM. Missing the target: matrix metalloproteinase antitargets in inflammation and cancer. *Trends Pharmacol Sci* 2013;**34**(4):233–42.
72. Shay G et al. Selective inhibition of matrix metalloproteinase-2 in the multiple myeloma-bone microenvironment. *Oncotarget* 2017;**8**(26):41827–40.
73. Tauro M et al. Bone seeking matrix metalloproteinase-2 inhibitors prevent bone metastatic breast cancer growth. *Mol Cancer Ther* 2017.